CHEMISTRY OF MATERIALS

Article

pubs.acs.org/cm

Large Negative Thermal Expansion and Anomalous Behavior on Compression in Cubic ReO_3-Type $A^{II}B^{IV}F_6$: $CaZrF_6$ and $CaHfF_6$

Justin C. Hancock,[†] Karena W. Chapman,[‡] Gregory J. Halder,[‡] Cody R. Morelock,[†] Benjamin S. Kaplan,[†] Leighanne C. Gallington,[†] Angelo Bongiorno,[†,§] Chu Han,[†] Si Zhou,[§] and Angus P. Wilkinson*[,†,#]

[†]School of Chemistry and Biochemistry, Georgia Institute of Technology, Atlanta, Georgia 30332-0400, United States

[‡]X-ray Science Division, Advanced Photon Source, Argonne National Laboratory, Lemont, Illinois 60439, United States

[§]School of Physics, Georgia Institute of Technology, Atlanta, Georgia 30332-0430, United States

[#]School of Materials Science and Engineering, Georgia Institute of Technology, Atlanta, Georgia 30332-0245, United States

Supporting Information

ABSTRACT: $CaZrF_6$ and $CaHfF_6$ display much stronger negative thermal expansion (NTE) ($\alpha_{L100\ K} \sim -18$ and -22 ppm·K^{-1}, respectively) than ZrW_2O_8 and other corner-shared framework structures. Their NTE is comparable to that reported for framework solids containing multiatom bridges, such as metal cyanides and metal−organic frameworks. However, they are formable as ceramics, transparent over a wide wavelength range and can be handled in air; these characteristics can be beneficial for applications. The NTE of $CaZrF_6$ is strongly temperature-dependent, and first-principles calculations show that it is largely driven by vibrational modes below ~150 cm^{-1}. $CaZrF_6$ is elastically soft with a bulk modulus (K_{300K}) of 37 GPa and, upon compression, starts to disorder at ~400 MPa. The strong NTE of $CaZrF_6$, which remains cubic to <10 K, contrasts with cubic $CoZrF_6$, which only displays modest NTE above its rhombohedral to cubic phase transition at ~270 K. $CaZrF_6$ and $CaHfF_6$ belong to a large and compositionally diverse family of materials, $A^{II}B^{IV}F_6$, providing for a detailed exploration of the chemical and structural factors controlling NTE and many opportunities for the design of controlled thermal expansion materials.

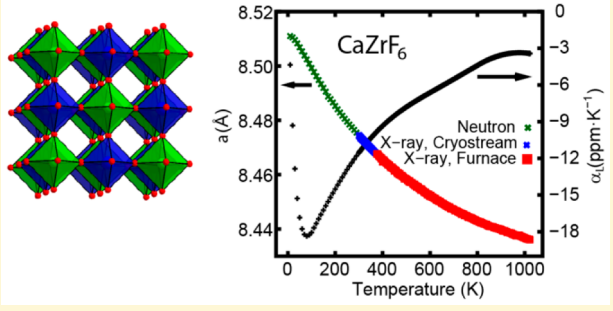

1. INTRODUCTION

Few materials display strong volume negative thermal expansion (NTE) over a large temperature range. The long-time leading NTE exemplar was ZrW_2O_8,[1] in which NTE arises from low-frequency vibrations involving the correlated motion of corner-shared framework polyhedra.[2,3] ZrW_2O_8 and other materials displaying strong NTE have attracted considerable attention because of the rarity of the phenomenon and the possibility of using them to compensate for the positive thermal expansion of other materials either in expansion-controlled composites or as separate components.[4] To move significantly beyond the expansion characteristics of ZrW_2O_8[1] and other oxide frameworks, solids with spatially extended links between structural units or alternative mechanisms for their NTE have been pursued. This has resulted in the discovery of very strong NTE because of vibrations in metal−organic frameworks (MOFs) with carboxylate links[5,6] and cyanide-bridged frameworks[7−9] and materials where magnetostrictive[10,11] or electronic[12,13] mechanisms operate. For potential application, NTE materials need to be stable under the conditions of use and amenable to the fabrication of composites or bulk components. Both MOFs and cyanide-bridged frameworks are not readily processed into ceramic bodies, and MOFs only display NTE when carefully evacuated to remove guests, such as atmospheric moisture, from their pore systems.

Metal fluorides are known to adopt structures analogous to those of oxides. However, the more ionic character of the M−F bonding can lead to very different thermophysical properties. In an early study of NTE in fluorides, we reported that ScF_3, which has a very simple ReO_3-type structure and remains cubic to <10 K,[14] displays strong NTE over a wide temperature range.[14] As they can provide good optical transparency into the IR and be fabricated in ceramic form, metal fluorides with atypical thermal expansion characteristics have potential for application in optics. Notably, fluorozirconate glasses, such as ZBLAN (ZrF_4−BaF_2−LaF_3−AlF_3−NaF) compositions, are used in IR-transparent optical fibers, but these glasses display strong positive thermal expansion.[15] Efforts to tune the thermal expansion of ScF_3 while maintaining transparency have met with limited success,[16−19] and all other ReO_3-connectivity $M^{III}F_3$ are unstable on cooling with respect to a structural phase transition, which results in strong positive volume thermal expansion below the transition temperature. This symmetry-

Received: February 19, 2015
Revised: May 6, 2015
Published: May 6, 2015

DOI: 10.1021/acs.chemmater.5b00662
Chem. Mater. 2015, 27, 3912−3918

lowering transition is typically associated with vibrational mode softening at the R-point, and in ScF_3, this same mode makes a major contribution to its NTE.[20]

While the number of simple $M^{III}F_3$ with ReO_3-connectivity is limited, there are many $A^{II}B^{IV}F_6$ compositions that adopt rock salt cation-ordered ReO_3-type structures (Figure 1).[21−23]

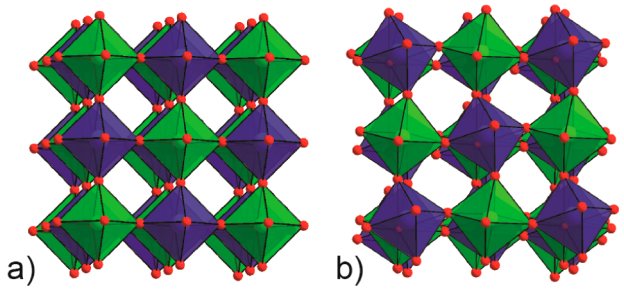

Figure 1. Crystal structures of cation-ordered $A^{II}B^{IV}F_6$ in their (a) cubic ($Fm\bar{3}m$) and (b) rhombohedral ($R\bar{3}$) forms.

Several of these maintain cubic symmetry, which is necessary for strong NTE, to low temperature. The thermal expansion of this family of materials has received little attention, but the limited data available for $CoZrF_6$, immediately above a rhombohedral ($R\bar{3}$) to cubic ($Fm\bar{3}m$) phase transition, show that its expansion coefficient is close to zero at room temperature.[24] Our observation that the highly ionic ScF_3 remains cubic to <10 K and displays strong NTE over a wide temperature range[14] motivated the present study of $CaZrF_6$ and $CaHfF_6$, which are also both highly ionic, and a comparison of their behavior to that of $CoZrF_6$ and ScF_3. In this paper, we examine the remarkable behavior of $CaZrF_6$ as a function of temperature and pressure, using diffraction methods, and complement these studies with first-principles calculations of vibrational modes.

2. EXPERIMENTAL SECTION

$M^{(II)}(Zr/Hf)F_6$ was prepared via the solid-state reaction of $M^{(II)}F_2$ and ZrF_4/HfF_4 powders. For the synthesis of $CaZrF_6$, $CaHfF_6$, and $CoZrF_6$, the starting materials were mixed in a 1:1 molar ratio. The powders were mixed and pelletized under a dry nitrogen atmosphere, and each sample was placed into either a copper tube ($CoZrF_6$) or a nickel tube ($CaZrF_6$ and $CaZrF_6$). The ends of the metal tubes were sealed by arc-welding under an argon atmosphere, and then the tubes were placed in an evacuated quartz ampule. The ampules were heated for 24 h at 750 °C for the synthesis of $CaZrF_6$ and at 850 °C for the syntheses of $CaHfF_6$ and $CoZrF_6$. The products were cooled slowly to room temperature using a 12 h ramp for $CaZrF_6$ and $CaZrF_6$ and using a 3 h ramp for $CoZrF_6$.

All sample handling/preparation for the diffraction measurements was performed in an inert atmosphere glovebox (neutron) or glovebag (X-ray). Neutron powder diffraction measurements were performed using the PAC sample environment on the POWGEN instrument at the Spallation Neutron Source, Oak Ridge National Laboratory. Low- and high-temperature X-ray powder diffraction measurements were performed using an Oxford Cryosystems Cryostream (100−500 K) and a resistively heated furnace (350−1173 K) on the 17-BM beamline at the Advanced Photon Source, Argonne National Laboratory. High-pressure X-ray diffraction data (298 K and P < ∼1.5 GPa) were recorded at 17-BM for a sample contained in an EasyLab "Diacell Bragg-(G)" diaphragm diamond anvil cell (DAC) while the pressure was continuously increased. Pressure was determined using Bragg peaks from NaCl, which was mixed with the sample prior to loading the DAC, and the Birch equation of state for NaCl.[25] Alfa silicone oil, with a molecular weight of 237 $g{\cdot}mol^{-1}$, was used as a pressure-transmitting fluid. High-pressure X-ray diffraction data were also recorded at the 11-ID-B beamline of the Advanced Photon Source between 298 and 523 K at precisely controlled pressures up to 310 MPa, using a heated titanium pressure vessel and background reducing internal mask (BRIM)[26] as described previously.[16] Infrared spectroscopic measurements were made using a Bruker Alpha Fourier transform infrared (FT-IR) spectrometer equipped with an attenuated total reflection (ATR) module.

Density functional theory calculations were carried out with software provided in the QUANTUM-Espresso toolkit.[27] Calculations were performed using a plane-wave energy cutoff of 160 Ry, norm-conserving pseudopotentials (valence electron configurations: Ca [$3s^23p^64s^2$], Zr [$4s^24p^64d^25s^2$], F [$2s^22p^5$]),[28] and a generalized gradient approximation of the exchange and correlation energy functional.[29] The PWscf code was used to perform total energy calculations and structural optimizations, while the Phonon code was used to compute phonon frequencies. We obtained a lattice parameter and a bulk modulus for $CaZrF_6$ at 0 K and 0 MPa equal to 8.78 Å and 51.7 GPa, respectively. The difference between the calculated and experimental lattice constant at low temperature is ∼3%, which is within the limits of agreement typically reached by this type of calculation. Mode Grüneisen parameters, which are indicative of a vibrational mode's contribution to thermal expansion,[30] were calculated via numerical differentiation. Phonon frequencies for $CaZrF_6$ were calculated at the equilibrium volume for 0 K and 0 MPa and with a reduction in lattice constant of up to 0.06% corresponding to a pressure of ∼100 MPa.

3. RESULTS AND DISCUSSION

3.1. Thermal Expansion of Cubic $CaZrF_6$ and $CaHfF_6$.

Rietveld analyses of neutron diffraction data (10−300 K), using the reported structure of cubic $CoZrF_6$[24] as a starting point, for $CaZrF_6$ and $CaHfF_6$ revealed that both remain cubic down to at least 10 K and display very strong NTE. A similar stability against distortion on cooling was previously observed for ScF_3 and is probably associated with the increase in electrostatic repulsion between like-charged ions on distortion of these highly ionic fluorides.[14] The observed NTE for $CaZrF_6$ and $CaHfF_6$ (Figure 2) is significantly greater in magnitude than that for ScF_3 (α_l ∼ −14 and −8 $ppmK^{-1}$ at 100 and 300 K, respectively) and is comparable to that reported for framework solids containing multiatom bridges, such as cyanides[7−9] and MOFs.[5,6]

Their low-temperature linear coefficients of thermal expansion are highly temperature-dependent (Figure 2), with minima at ∼100 K and a rapid rise to zero below 50 K, as required by thermodynamics. The temperature dependence above 100 K is significantly greater than that reported for $Zn(CN)_2$[8] and MOF-5.[6] The thermal expansion of $CaZrF_6$ and $CaHfF_6$, which are structurally and chemically very similar, appear to be somewhat different, although the significant scatter in the CTE values for $CaHf_6$ complicates their interpretation. The hafnium compound apparently shows a less rapid increase in the magnitude of its NTE at very low temperatures but a

DOI: 10.1021/acs.chemmater.5b00662
Chem. Mater. 2015, 27, 3912−3918

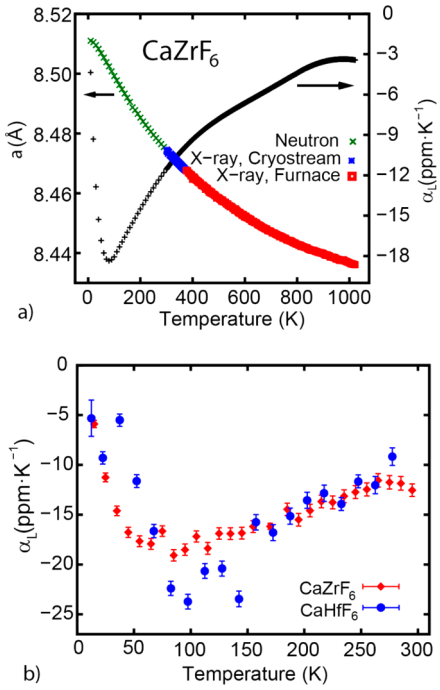

Figure 2. Thermal expansion characteristics of $CaZrF_6$ and $CaHfF_6$; (a) lattice constant and derived linear expansion coefficients for $CaZrF_6$ and (b) a comparison of the low-temperature thermal expansion in $CaZrF_6$ and $CaHfF_6$. In a, the temperature dependence of the expansion coefficient was determined from polynomial fits to the lattice constant versus temperature, but in b, it was determined by taking differences between lattice constants at closely spaced temperatures.

greater magnitude by ~100 K. Analyses of X-ray powder diffraction data collected for $CaZrF_6$ in the range 100−1173 K show that its coefficient of thermal expansion rises (Figure 2a) almost monotonically with temperature between 400 and 800 K, reaching −4 ppm·K^{-1} at 900 K. Above 900 K, products from sample decomposition or from reaction with the fused silica sample tube become apparent in the X-ray data (Figure S2 of the Supporting Information), but some $CaZrF_6$ persists until ~1050 K, which is above the temperature used for its synthesis. The strong temperature dependence of the coefficient of thermal expansion must reflect increasing contributions from vibrational modes with positive Grüneisen parameters compensating for the contribution from low-energy modes with negative parameters. This may be a general characteristic of fluorides that show strong NTE at low temperatures, as all the vibrational modes, including those that contribute to bond elongation, are at low frequency because of the relatively low force constants associated with ionic metal fluoride bonds.

In NTE framework solids, such as $CaZrF_6$, the true M−X bond lengths are expected to increase on heating, with the NTE arising from transverse thermal motion of bridging species (see later). However, the apparent M−X bond lengths, derived from the crystallographic coordinates without taking into account correlated thermal motion, often decrease on heating, see for example Evans et al.[31] The neutron diffraction analyses for cubic $CaZrF_6$ show that the apparent Ca−F and Zr−F bond lengths decrease in a similar fashion on heating from 10 to 300 K. However, analyses of the X-ray data suggest that in the high-temperature regime the apparent Zr−F bond lengths continue to decrease on heating, but those for Ca−F start to increase.

The nature of the low-frequency vibrational modes underpinning NTE in ZrW_2O_8,[2,3] $M(CN)_2$ (M: Zn, Cd),[32] and MOF-5[33] has been the subject of considerable recent interest. While early work focused on the transverse displacement of anions and the rocking of rigid structural units,[34] a more complex picture involving correlated rotations, translations, and distortions of structural building units has emerged in some cases.[2,3,35] The atomic displacement parameters derived from the neutron diffraction data for $CaZrF_6$ (Figure S3 of the Supporting Information) show a strong temperature dependence for the component associated with fluoride motion perpendicular to the Ca−F−Zr vector (U_{33}); this behavior is consistent with a rigid unit mode (RUM) polyhedral rocking mechanism for NTE,[34] but the apparent difference in expansion between $CaZrF_6$ and $CaHfF_6$ (Figure 2b) suggests that some modes contributing to the NTE may involve the displacement of Zr/Hf, as the different masses of these elements would not otherwise be expected to play a role. For simple solids, the temperature dependence of atomic displacement parameters and their values at 0 K can be used to estimate a material's Debye temperature.[36] An analysis of this type for $CaZrF_6$, applied solely to U_{33} for fluoride, suggests a Debye temperature of ~220 K, which is comparable to the energy of the vibrations with the largest negative contributions to thermal expansion (see below).

Phonon dispersion curves for cubic $CaZrF_6$ (Figure 3a), calculated using a density-functional perturbation theory

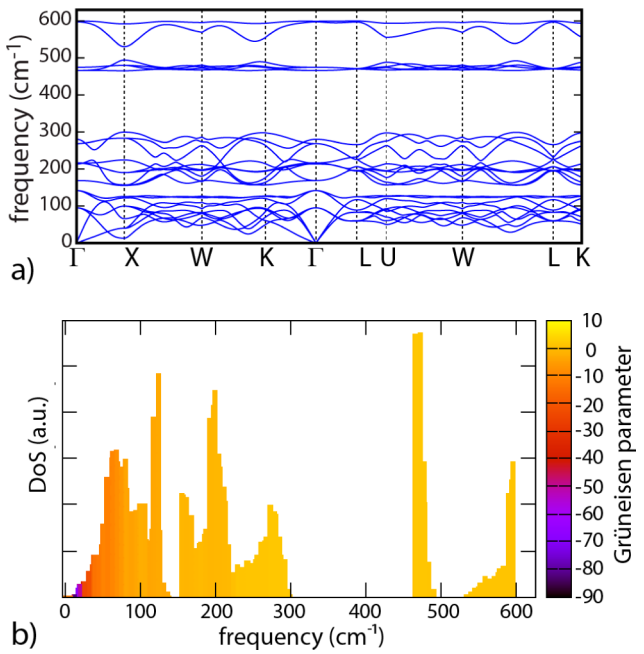

Figure 3. Results from ab initio calculations of phonons in $CaZrF_6$; (a) phonon dispersion curves and (b) the phonon density of states, color coded by average mode Grüneisen parameter at each frequency.

approach,[27] show that all modes have positive frequencies, which is consistent with the absence of a structural phase transition on cooling to 10 K. There are no modes above 620 cm^{-1}, in agreement with reflectance IR measurements (Figure S6 of the Supporting Information), which show the main onset of absorption at ~650 cm^{-1} (corresponding to ~15 μm or ~80 meV). Mode Grüneisen parameters, derived from the calculated change in phonon frequency on compression,

DOI: 10.1021/acs.chemmater.5b00662
Chem. Mater. 2015, 27, 3912−3918

indicate that both the low dispersion modes in the range 500−620 cm^{-1} and the highest energy modes around 250 cm^{-1} make positive contributions to the material's thermal expansion, as they have predominantly positive Grüneisen parameters. The most strongly negative Grüneisen parameters (Figure 3b) are associated with modes below ∼150 cm^{-1} (∼215 K). There are negative contributions from modes across the entire Brillouin zone, but the most negative Grüneisen parameters are associated with modes close to the X point. This behavior somewhat contrasts that of ScF_3, in which low-frequency modes close to the R point make major contributions to NTE, including the soft mode that is responsible for its cubic-to-rhombohedral transition on compression.[20]

3.2. Thermal Expansion and Phase Transitions of $CoZrF_6$. The strong NTE shown by cubic $CaZrF_6$ and $CaHfF_6$ contrasts with the behavior of $CoZrF_6$. X-ray powder diffraction measurements on $CoZrF_6$ show strong positive volume thermal expansion below the $R\bar{3}$ to $Fm\bar{3}m$ phase transition (∼270 K), followed by low positive thermal expansion immediately above the transition and modest NTE at higher temperatures (Figure 4). In the $R\bar{3}$ phase, the expansion is highly anisotropic (Figure S4 of the Supporting Information). The lowest expansion coefficient for $CoZrF_6$ ($\alpha_l \sim -3$ ppm·K^{-1}) occurs at ∼400 K, but at this temperature, the corresponding value for $CaZrF_6$ is ∼−9 ppm·K^{-1}. Diffuse scattering in a single-crystal X-ray photograph of $CoZrF_6$ at 300 K[24] suggests that the cubic phase contains local distortions away from the ideal ReO_3-type structure, which could make positive contributions to the thermal expansion. At 400 K, the difference in expansion between $CoZrF_6$ and $CaZrF_6$ presumably arises because the potentials underlying the lattice vibrations of these materials are different; the observed distortion to lower symmetry on cooling implies that cubic $CoZrF_6$ has a potential with multiple minima for some distortion coordinates, but $CaZrF_6$ does not. We believe that the highly ionic bonding in $CaZrF_6$, when compared to $CoZrF_6$, plays an important role in stabilizing its cubic structure against distortion, even at very low temperatures, as such a distortion brings ions of the same charge closer together.

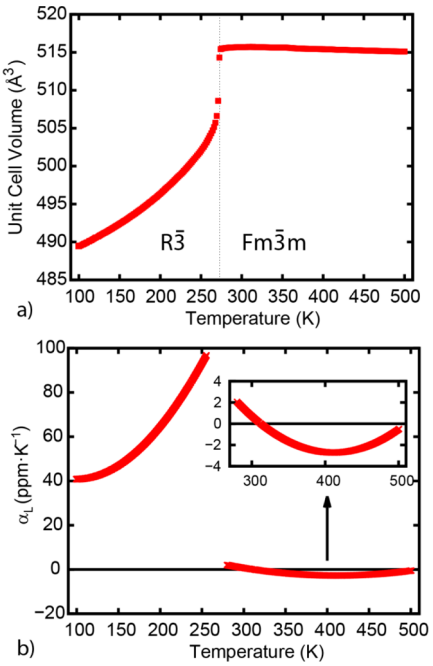

Figure 4. Thermal expansion characteristics of $CoZrF_6$. (a) Unit cell volume and (b) average linear expansion coefficient versus temperature. The CTE was determined from a polynomial fit to the volume versus temperature.

3.3. Behavior of $CaZrF_6$ at High Pressure. The behavior of NTE materials upon compression is of practical and fundamental importance. If used in composites, NTE materials experience stresses because of thermal expansion mismatch that can change physical properties and even cause phase transitions.[37,38] The same mode softening on volume reduction that gives rise to negative Grüneisen parameters, and hence NTE, can also ultimately lead to structural phase transitions on compression. Consequently, many NTE materials display rich behavior on compression; crystal-to-crystal phase transitions at <1 GPa are common, and some materials amorphize.[39]

Like many NTE materials, $CaZrF_6$ is sensitive to stress but, unlike ScF_3, does not undergo a simple displacive cubic to rhombohedral symmetry-lowering phase transition on compression.[14] Measurements in a DAC at room temperature (Figure 5) show the onset of a phase transition at around 400 MPa that leads to a low crystallinity, or amorphous, material that persists on decompression. As both calcium and zirconium often occur with higher coordination numbers than in cubic $CaZrF_6$, the loss of long-range order may be associated with an increase in coordination number. An analysis of the diffraction data recorded in a DAC below 400 MPa indicates that cubic $CaZrF_6$ is elastically soft, with a bulk modulus of ∼36 GPa at ∼300 K. This value is lower than that estimated in our ab initio calculations (∼51 GPa), but the difference could arise in part because the first-principles estimate does not take into account the effects of temperature, and some NTE materials are known to show considerable softening on heating.[40]

Most materials stiffen on compression, as the increase in density leads to enhanced repulsions between atoms, and soften on heating. However, ZrW_2O_8[41] and $Zn(CN)_2$[42] are known to display pressure-induced softening, resulting in negative values for the pressure derivative of the bulk modulus, K_0'. In the case of $Zn(CN)_2$, this phenomenon is temperature-dependent.[43] As recent work suggests that temperature-dependent pressure-induced softening may be common among NTE materials[44] and that it is intimately tied to their NTE,[45] the effects of temperature and pressure on the bulk modulus of $CaZrF_6$ were explored over the range 298−514 K and pressures <0.31 GPa. A series of straight-line fits to the resulting pressure/volume data, over the range 50−310 MPa, indicate thermal softening, with the average bulk moduli dropping from 37 to 34 GPa between 298 and 514 K. There is a corresponding small increase in the magnitude of the NTE on compression, with $\alpha_{l(298-514\ K)}$ changing from −9.2 ppm·K^{-1} at 50 MPa to −9.9 ppm·K^{-1} at 310 MPa. An examination of the change in volume on compression at 298 K suggests a softening (Figure S5a of the Supporting Information). A fit using a third-order Birch−Murnaghan equation of state (EoS), with EoSFit7,[46] to these data resulted in estimates for the bulk modulus, K_0, and its pressure derivative, K_0', of 42.1(8) GPa and −26(4), respectively. However, fits to data from higher temperatures showed considerable scatter in the estimated K_0', presumably because of the limited pressure range of the experiment combined with the uncertainties in the estimated pressures and volumes. To better control these uncertainties, a single fit, making simultaneous use of all available PVT data (Table S5 of the Supporting Information), to a third-order Birch−

DOI: 10.1021/acs.chemmater.5b00662
Chem. Mater. 2015, 27, 3912−3918

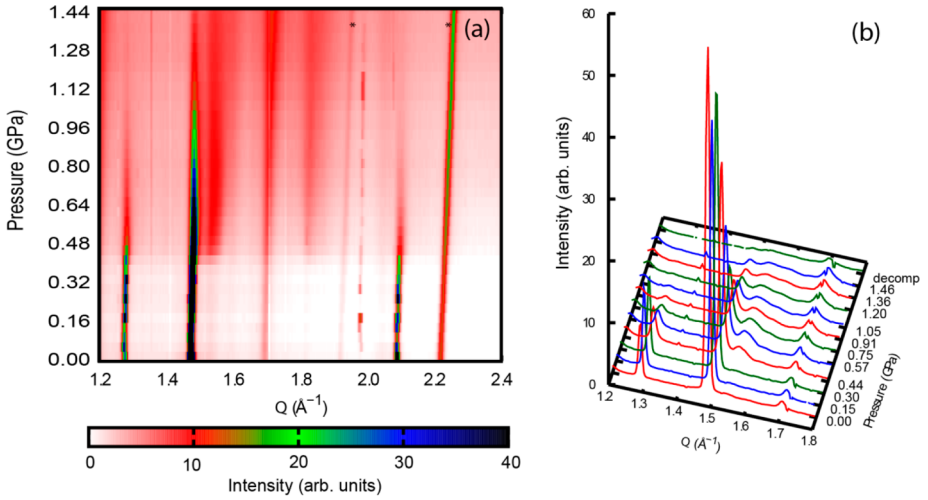

Figure 5. (a) Powder X-ray diffraction data for $CaZrF_6$ upon compression in a diamond anvil cell using a NaCl pressure calibrant (*). (b) The major Bragg peaks from $CaZrF_6$ begin to disappear at ∼400 MPa, and a disordered product remains on decompression. The peak at ∼1.7 Å^{-1} is from an impurity.

Murnaghan EoS and the Berman model for temperature-dependent thermal expansion was performed in EoSFit7.[46] This led to the following EoS parameters: K_{298K} = 39.2(7) GPa, K_{298K}' = −13(3), dK/dT = −0.012(2) GPa·K^{-1}, α_0 = −3.28(6) × 10^{-5}, and α_1 = 4.2(5), supporting the occurrence of both a pressure and thermally induced softening in $CaZrF_6$, in the pressure−temperature range examined. A 1-D version of the ReO_3 structure has been used to predict the behavior of K_0' in NTE solids.[47]

3.4. Moisture Stability. Many metal fluorides are moisture-reactive, including ZBLAN and related glass compositions.[48] However, both IR spectroscopic measurements (Figure S6 of the Supporting Information) and X-ray powder diffraction experiments for $CaZrF_6$ indicate that it can be handled in air. Poor stability in the presence of moisture may limit the potential for application of some $A^{II}B^{IV}F_6$ compositions.

4. CONCLUSIONS

Highly ionic $CaZrF_6$ and $CaHfF_6$ remain cubic to very low temperatures and show very strong NTE over a wide temperature range. This expansion behavior contrasts with that of $CoZrF_6$, which shows a symmetry-lowering phase transition on cooling. $CaZrF_6$ and $CaHfF_6$ are members of a large $A^{II}B^{IV}F_6$ family, providing for a detailed exploration of the chemical and structural factors controlling NTE, and many opportunities for the design of controlled thermal expansion materials. As these fluorides are optically transparent over a wide wavelength range and can be fabricated in ceramic form, the design of thermally stable IR optical components based on $A^{II}B^{IV}F_6$ compositions can be readily envisaged.

■ ASSOCIATED CONTENT

Supporting Information

Example Rietveld fits, plot showing diffraction data for $CaZrF_6$ as a function of temperature, atomic displacement parameters for $CaZrF_6$ as a function of temperature, plot showing lattice constants versus temperature for $CoZrF_6$, plot showing volume versus pressure for $CaZrF_6$, plot showing bulk modulus versus temperature for $CaZrF_6$, FTIR ATR spectrum of $CaZrF_6$, tables of lattice constants versus temperature for $CaZrF_6$, $CaHfF_6$, and $CoZrF_6$. The Supporting Information is available free of charge on the ACS Publications website at DOI: 10.1021/acs.chemmater.5b00662.

■ AUTHOR INFORMATION

Corresponding Author

*E-mail: angus.wilkinson@chemistry.gatech.edu.

Notes

The authors declare no competing financial interests.

■ ACKNOWLEDGMENTS

We are grateful for support from the Georgia Institute of Technology including a President's Undergraduate Research Award. Experiments were performed at the Advanced Photon Source, a U.S. Department of Energy (DOE) Office of Science User Facility operated for the DOE Office of Science by Argonne National Laboratory under Contract No. DE-AC02-06CH11357. We are grateful for experimental assistance from the scientific staff on the POWGEN instrument at SNS. Experiments were also conducted at ORNL's Spallation Neutron Source, which is sponsored by the Scientific User Facilities Division, Office of Basic Energy Sciences, U.S. Department of Energy.

■ REFERENCES

(1) Mary, T. A.; Evans, J. S. O.; Vogt, T.; Sleight, A. W. Negative Thermal Expansion from 0.3 to 1050 Kelvin in ZrW_2O_8. *Science* **1996**, *272*, 90.

(2) Gupta, M. K.; Mittal, R.; Chaplot, S. L. Negative Thermal Expansion in Cubic ZrW_2O_8: Role of Phonons in the Entire Brillouin Zone from Ab Initio Calculations. *Phys. Rev. B* **2013**, *88*, 014303.

(3) Bridges, F.; Keiber, T.; Juhas, P.; Billinge, S. J. L.; Sutton, L.; Wilde, J.; Kowach, G. R. Local Vibrations and Negative Thermal Expansion in ZrW_2O_8. *Phys. Rev. Lett.* **2014**, *112*, 045505.

(4) Romao, C. P.; Miller, K. J.; Whitman, C. A.; White, M. A.; Marinkovic, B. A. In *Comprehensive Inorganic Chemistry II*; Reedijk, J., Poeppelmeier, K. R., Eds.; Elsevier: Oxford, 2013; Vol. *4*, p 128.

(5) Dubbeldam, D.; Walton, K. S.; Ellis, D. E.; Snurr, R. Q. Exceptional Negative Thermal Expansion in Isoreticular Metal-Organic Frameworks. *Angew. Chem., Int. Ed.* **2007**, *46*, 4496.

(6) Zhou, W.; Wu, H.; Yildirim, T.; Simpson, J. R.; Walker, A. R. H. Origin of the Exceptional Negative Thermal Expansion in Metal-Organic Framework-5 Zn_4O(1,4-Benzenedicarboxylate)$_3$. *Phys. Rev. B* **2008**, *78*, 054114.

DOI: 10.1021/acs.chemmater.5b00662
Chem. Mater. 2015, 27, 3912−3918

(7) Phillips, A. E.; Goodwin, A. L.; Halder, G. J.; Southon, P. D.; Kepert, C. J. Nanoporosity and Exceptional Negative Thermal Expansion in Single-Network Cadmium Cyanide. *Angew. Chem., Int. Ed.* **2008**, *47*, 1396.
(8) Goodwin, A. L.; Kepert, C. J. Negative Thermal Expansion and Low-Frequency Modes in Cyanide-Bridged Framework Materials. *Phys. Rev. B* **2005**, *71*, 140301.
(9) Chapman, K. W.; Chupas, P. J.; Kepert, C. J. Direct Observation of a Transverse Vibrational Mechanism for Negative Thermal Expansion in $Zn(CN)_2$: An Atomic Pair Distribution Function Analysis. *J. Am. Chem. Soc.* **2005**, *127*, 15630.
(10) Iikubo, S.; Kodama, K.; Takenaka, K.; Takagi, H.; Takigawa, M.; Shamoto, S. Local Lattice Distortion in the Giant Negative Thermal Expansion Material $Mn_3Cu_{1-X}Ge_xN$. *Phys. Rev. Lett.* **2008**, *101*, 205901.
(11) Huang, R.; Liu, Y.; Fan, W.; Tan, J.; Xiao, F.; Qian, L.; Li, L. Giant Negative Thermal Expansion in $NaZn_{13}$-Type $La(Fe, Si, Co)_{13}$ Compounds. *J. Am. Chem. Soc.* **2013**, *135*, 11469.
(12) Azuma, M.; Chen, W. T.; Seki, H.; Czapski, M.; Olga, S.; Oka, K.; Mizumaki, M.; Watanuki, T.; Ishimatsu, N.; Kawamura, N.; Ishiwata, S.; Tucker, M. G.; Shimakawa, Y.; Attfield, J. P. Colossal Negative Thermal Expansion in $BiNiO_3$ Induced by Intermetallic Charge Transfer. *Nat. Commun.* **2011**, *2*, 1.
(13) Long, Y. W.; Hayashi, N.; Saito, T.; Azuma, M.; Muranaka, S.; Shimakawa, Y. Temperature-Induced a-B Intersite Charge Transfer in an a-Site-Ordered $LaCu_3Fe_4O_{12}$ Perovskite. *Nature* **2009**, *458*, 60.
(14) Greve, B. K.; Martin, K. L.; Lee, P. L.; Chupas, P. J.; Chapman, K. W.; Wilkinson, A. P. Pronounced Negative Thermal Expansion from a Simple Structure: Cubic ScF_3. *J. Am. Chem. Soc.* **2010**, *132*, 15496.
(15) Adam, J. L. Lanthanides in Non-Oxide Glasses. *Chem. Rev.* **2002**, *102*, 2461.
(16) Morelock, C. R.; Greve, B. K.; Gallington, L. C.; Chapman, K. W.; Wilkinson, A. P. Negative Thermal Expansion and Compressibility of $Sc_{1-x}Y_xF_3$ ($x < 0.25$). *J. Appl. Phys.* **2013**, *114*, 213501.
(17) Morelock, C. R.; Gallington, L. C.; Wilkinson, A. P. Evolution of Negative Thermal Expansion and Phase Transitions in $Sc_{1-x}Ti_xF_3$. *Chem. Mater.* **2014**, *26*, 1936.
(18) Morelock, C. R.; Gallington, L. C.; Wilkinson, A. P. Solid Solubility, Phase Transitions, Thermal Expansion, and Compressibility in $Sc_{1-x}Al_xF_3$. *J. Solid State Chem.* **2015**, *222*, 96.
(19) Hu, L.; Chen, J.; Fan, L.; Ren, Y.; Rong, Y.; Pan, Z.; Deng, J.; Yu, R.; Xing, X. Zero Thermal Expansion and Ferromagnetism in Cubic $Sc_{1-x}M_xF_3$ (M = Ga, Fe) over a Wide Temperature Range. *J. Am. Chem. Soc.* **2014**, *136*, 13566.
(20) Li, C. W.; Tang, X.; Muñoz, J. A.; Keith, J. B.; Tracy, S. J.; Abernathy, D. L.; Fultz, B. Structural Relationship between Negative Thermal Expansion and Quartic Anharmonicity of Cubic ScF_3. *Phys. Rev. Lett.* **2011**, *107*, 195504.
(21) Reinen, D.; Steffens, F. Structure and Bonding in Transition-Metal Fluorides $M^{II}Me^{IV}F_6$. A. Phase-Transitions. *Z. Anorg. Allg. Chem.* **1978**, *441*, 63.
(22) Babel, D.; Tressaud, A. In *Inorganic Solid Fluorides*; Hagenmuller, P., Ed.; Academic Press, Inc.: Orlando, FL, 1985; p 78.
(23) Leblanc, M.; Maisonneuve, V.; Tressaud, A. Crystal Chemistry and Selected Physical Properties of Inorganic Fluorides and Oxide-Fluorides. *Chem. Rev.* **2015**, *115*, 1191.
(24) Rodriguez, V.; Couzi, M.; Tressaud, A.; Grannec, J.; Chaminade, J. P.; Soubeyroux, J. L. Structural Phase-Transition in the Ordered Fluorides $M^{II}ZrF_6$ (M^{II} = Co, Zn). 1. Structural Study. *J. Phys.: Condens. Matter* **1990**, *2*, 7373.
(25) Birch, F. Equation of State and Thermodynamic Parameters of Sodium Chloride to 300 Kbar in the High-Temperature Domain. *J. Geophys. Res. B* **1986**, *91*, 4949.
(26) Wilkinson, A. P.; Morelock, C. R.; Greve, B. K.; Jupe, A. C.; Chapman, K. W.; Chupas, P. J.; Kurtz, C. Reducing the Background from Pressure Vessels Using a BRIM. *J. Appl. Crystallogr.* **2011**, *44*, 1047.
(27) Giannozzi, P.; Baroni, S.; Bonini, N.; Calandra, M.; Car, R.; Cavazzoni, C.; Ceresoli, D.; Chiarotti, G. L.; Cococcioni, M.; Dabo, I.; Dal Corso, A.; de Gironcoli, S.; Fabris, S.; Fratesi, G.; Gebauer, R.; Gerstmann, U.; Gougoussis, C.; Kokalj, A.; Lazzeri, M.; Martin-Samos, L.; Marzari, N.; Mauri, F.; Mazzarello, R.; Paolini, S.; Pasquarello, A.; Paulatto, L.; Sbraccia, C.; Scandolo, S.; Sclauzero, G.; Seitsonen, A. P.; Smogunov, A.; Umari, P.; Wentzcovitch, R. M. Quantum Espresso: A Modular and Open-Source Software Project for Quantum Simulations of Materials. *J. Phys.: Condens. Matter* **2009**, *21*, 395502.
(28) Troullier, N.; Martins, J. L. Efficient Pseudopotentials for Plane-Wave Calculations. *Phys. Rev. B* **1991**, *43*, 1993.
(29) Perdew, J. P.; Burke, K.; Ernzerhof, M. Generalized Gradient Approximation Made Simple. *Phys. Rev. Lett.* **1996**, *77*, 3865.
(30) Barrera, G. D.; Bruno, J. A. O.; Barron, T. H. K.; Allan, N. L. Negative Thermal Expansion. *J. Phys.: Condens. Matter* **2005**, *17*, R217.
(31) Evans, J. S. O.; Mary, T. A.; Sleight, A. W. Negative Thermal Expansion in $Sc_2(WO_4)_3$. *J. Solid State Chem.* **1998**, *137*, 148.
(32) Ding, P.; Liang, E. J.; Jia, Y.; Du, Z. Y. Electronic Structure, Bonding and Phonon Modes in the Negative Thermal Expansion Materials of $Cd(CN)_2$ and $Zn(CN)_2$. *J. Phys.: Condens. Matter* **2008**, *20*, 275224.
(33) Lock, N.; Christensen, M.; Wu, Y.; Peterson, V. K.; Thomsen, M. K.; Piltz, R. O.; Ramirez-Cuesta, A. J.; McIntyre, G. J.; Noren, K.; Kutteh, R.; Kepert, C. J.; Kearley, G. J.; Iversen, B. B. Scrutinizing Negative Thermal Expansion in MOF-5 by Scattering Techniques and Ab Initio Calculations. *Dalton Trans.* **2013**, *42*, 1996.
(34) Tucker, M. G.; Goodwin, A. L.; Dove, M. T.; Keen, D. A.; Wells, S. A.; Evans, J. S. O. Negative Thermal Expansion in ZrW_2O_8: Mechanisms, Rigid Unit Modes, and Neutron Total Scattering. *Phys. Rev. Lett.* **2005**, *95*, 255501.
(35) Gava, V.; Martinotto, A. L.; Perottoni, C. A. First-Principles Mode Gruneisen Parameters and Negative Thermal Expansion in α-ZrW_2O_8. *Phys. Rev. Lett.* **2012**, *109*, 195503.
(36) Willis, B. T. M.; Prior, A. W. *Thermal Vibrations in Crystallography*; Cambridge University Press: Cambridge, U.K., 1975.
(37) Holzer, H.; Dunand, D. C. Phase Transformation and Thermal Expansion of Cu/ZrW_2O_8 Metal Matrix Composites. *J. Mater. Res.* **1999**, *14*, 780.
(38) Morelock, C. R.; Suchomel, M. R.; Wilkinson, A. P. A Cautionary Tale on the Use of GE-7031 Varnish: Low Temperature Thermal Expansion Studies of ScF_3. *J. Appl. Crystallogr.* **2013**, *46*, 823.
(39) Varga, T.; Wilkinson, A. P.; Jupe, A. C.; Lind, C.; Bassett, W. A.; Zha, C.-S. Pressure-Induced Amorphization of Cubic ZrW_2O_8 Studied in-Situ and Ex-Situ by Synchrotron X-Ray Absorption Spectroscopy and Diffraction. *Phys. Rev. B* **2005**, *72*, 024117.
(40) Drymiotis, F. R.; Ledbetter, H.; Betts, J. B.; Kimura, T.; Lashley, J. C.; Migliori, A.; Ramirez, A. P.; Kowach, G. R.; Van Duijin, J. Monocrystal Elastic Constants of the Negative-Thermal-Expansion Compound Zirconium Tungstate (ZrW_2O_8). *Phys. Rev. Lett.* **2004**, *93*, 025502.
(41) Pantea, C.; Migliori, A.; Littlewood, P. B.; Zhao, Y.; Ledbetter, H.; Lashley, J. C.; Kimura, T.; Van Duijn, J.; Kowach, G. R. Pressure-Induced Elastic Softening of Monocrystalline Zirconium Tungstate at 300 K. *Phys. Rev. B* **2006**, *73*.
(42) Chapman, K. W.; Chupas, P. J. Pressure Enhancement of Negative Thermal Expansion Behavior and Induced Framework Softening in Zinc Cyanide. *J. Am. Chem. Soc.* **2007**, *129*, 10090.
(43) Fang, H.; Phillips, A. E.; Dove, M. T.; Tucker, M. G.; Goodwin, A. L. Temperature-Dependent Pressure-Induced Softening in $Zn(CN)_2$. *Phys. Rev. B* **2013**, *88*, 144103.
(44) Fang, H.; Dove, M. T. Pressure-Induced Softening as a Common Feature of Framework Structures with Negative Thermal Expansion. *Phys. Rev. B* **2013**, *87*, 6.
(45) Fang, H.; Dove, M. T.; Phillips, A. E. Common Origin of Negative Thermal Expansion and Other Exotic Properties in Ceramic and Hybrid Materials. *Phys. Rev. B* **2014**, *89*, 214103.
(46) Angel, R. J.; Gonzalez-Platas, J.; Alvaro, M. EoSFit7c and a Fortran Module (Library) for Equation of State Calculations. *Z. Kristallogr.* **2014**, *229*, 405.
(47) Fang, H.; Dove, M. T. A Phenomenological Expression to Describe the Temperature Dependence of Pressure-Induced Softening

DOI: 10.1021/acs.chemmater.5b00662
Chem. Mater. 2015, 27, 3912−3918

in Negative Thermal Expansion Materials. *J. Phys.: Condens. Matter* **2014**, *26*, 5.
(48) Nazabal, V.; Poulain, M.; Olivier, M.; Pirasteh, P.; Camy, P.; Doualan, J. L.; Guy, S.; Djouama, T.; Boutarfaia, A.; Adam, J. L. Fluoride and Oxyfluoride Glasses for Optical Applications. *J. Fluorine Chem.* **2012**, *134*, 18.

DOI: 10.1021/acs.chemmater.5b00662
Chem. Mater. 2015, 27, 3912−3918